Volume-averaged conservation equations for volume-of-fluid interface tracking

M. Wörner[*], W. Sabisch, G. Grötzbach, D.G. Cacuci

Forschungszentrum Karlsruhe GmbH, Institut für Reaktorsicherheit,
Postfach 3640, 76021 Karlsruhe, Germany

Abstract

We derive local *volume-averaged* single-field conservation equations, called the VA-VOF equations, for a two-phase system consisting of two immiscible incompressible components. These equations are suitable for numerical simulations of dynamic interface evolutions with the Volume-of-Fluid (VOF) method, where the boundary layer at the interface is not fully resolved by the grid. As compared to the *local* equations currently used within the customary VOF-method, the newly derived mass and momentum conservation equations contain additional terms, which depend on the local phase-space-averaged relative velocity. For very fine grids, this relative velocity vanishes and the local form of the VOF equations is recovered. The additional terms in the VA-VOF equations are discussed and shown to render the VA-VOF equations incomplete. To close the VA-VOF equations, a local uniform relative velocity (LURV) model is presented. For a benchmark problem depicting a two-dimensional circular interface between two liquids in static equilibrium, the LURV-model is shown to reduce appreciably the negative effects of the spurious currents that numerically distort the interface.

1. Introduction

The Volume-of-Fluid (VOF) interface tracking method originally introduced by Hirt and Nichols (1981) is widely used for numerical simulation of immiscible and incompressible multi-fluid flows. Some recent applications of the VOF method include the rise of a gas bubble in a closed vertical cylinder (Chen et al., 1999), the impact of a single droplet against a solid surface (Bussmann et al., 1999) and on a liquid film (Rieber and Frohn, 1999), the breakup of a large bubble (Lawson et al., 1999), the bubble injection through a vent line in a water pool (Meier and Yadigaroglu, 2000), a pinching pendant drop (Gueyffier et al., 1999), and three-dimensional (3D) mold filling (Rider et al., 1998). The VOF method has also been applied to numerical simulations of flows in isothermal systems such as two-layer Couette flow, "bamboo waves" in vertical core-annular flow, drop breakup in shear flow (Li and Renardy, 2000), and other free-surface and interfacial flows (Scardovelli and Zaleski, 1999). Furthermore, Welch and Wilson (2000) used the VOF method to simulate numerically the phase-change in two-dimensional (2D) horizontal film boiling.

For a generic system consisting of two fluids, the VOF-method is mathematically based on a set of *local* equations involving the one-field assumption, in which *two* local mass and momentum conservation equations are replaced by *one* local mass and momentum conservation equation for the system's center-of-mass. As noted by Kothe (1998), the one-field model assumption is adequate when a representative volume element (RVE) does not contain homogeneous mixtures of the two fluids, since the RVEs are assumed to resolve the interface topology between the two fluids. In addition, the size of the RVEs should be sufficiently small to resolve the boundary layer at the interface; this is particularly important when the fluids are assumed to share the same velocity, as in VOF-formulations based on *local* equations. The requirement that the RVEs resolve the boundary layer may require much smaller RVEs than the requirement that they resolve the interface topology.

---

[*] Corresponding author. E-mail address: woerner@irs.fzk.de

Such considerations arise for physical systems where the difference between the velocities of the dispersed and continuous phases is large; a typical example is provided by bubbles rising at high Reynolds number in a stagnant liquid. Such problems cannot be solved efficiently with local equations discretized on fixed grids, as currently used for numerical simulations with the VOF methods, since the resolution of the boundary layer at the interface would require a much larger number of RVEs than would be necessary to resolve efficiently the interface topology.

Since all current VOF implementations are based on a set of *local* equations, it is essential that the boundary layer be fully resolved; otherwise, the use of local equations would become inappropriate because the velocity of each component would differ from the center-of mass velocity, giving rise to a non-zero drift velocity for each fluid. Using coarse computational grids for solving the *local* equations implies that zero drift velocities are assumed, which is equivalent to the use of a local "homogeneous model" for the phase velocities. This approximation must be carefully assessed when using coarse grid computations.

This paper presents a new, rigorous, formulation of the *locally volume-averaged single-field* mass and momentum conservation equations that describe the flow of two incompressible fluids. This formulation is suitable for VOF computations on coarse grids and does not *a priori* involve the assumption of zero local drift velocities. Consequently, the newly obtained conservation equations contain closure terms that depend on the local phase-space-averaged relative velocity ($\mathbf{v_r}$) between the phases. These terms arise in RVE's that instantaneously contain both phases.

The basis for our new formulation is provided by the volume-averaged two-field equations presented in section 2. The underlying mathematical derivations are highlighted in section 3. In section 4, we show that the newly formulated volume-averaged single-field mass and momentum conservation equations reduce to the well known local form used in current VOF methods when (i) the RVE's become vanishingly small, or (ii) the locally "homogeneous model" ($\mathbf{v_r} = 0$) holds or is presumed to hold. Section 5 presents a local algebraic model for $\mathbf{v_r}$ that closes the full set of equations. In particular, we investigate the influence of this model on the momentum equation by simulating a bubble in static equilibrium with the surrounding liquid. We note that this model reduces appreciably the negative effects of the so-called "spurious currents". Finally, section 6 presents a summary and conclusions.

2. Volume-averaged two-field equations

For easy reference, we summarize in this section the well-known derivation of the averaged equations for a two-fluid system (Ishii, 1975). Using the notations introduced by Drew and Passman (1999), we consider two isothermal fluids with densities ρ_1 and ρ_2, flowing with velocities $\mathbf{v}_1(\mathbf{x}, t)$ and $\mathbf{v}_2(\mathbf{x}, t)$, and residing in domains $\Omega_1(t)$ and $\Omega_2(t)$, respectively, such that $\Omega = \Omega_1(t) \bigcup \Omega_2(t) =$ constant. The local conservation equations for mass and momentum are:

$$\frac{\partial \rho_k}{\partial t} + \nabla \cdot \rho_k \mathbf{v_k} = 0 \qquad\qquad \mathbf{x} \in \Omega_k(t), \quad k \in 1,2 \qquad\qquad (1)$$

$$\frac{\partial \rho_k \mathbf{v_k}}{\partial t} + \nabla \cdot \rho_k \mathbf{v_k} \mathbf{v_k} = -\nabla p_k + \rho_k \mathbf{g} + \nabla \cdot \mathbf{\tau_k} \qquad \mathbf{x} \in \Omega_k(t), \quad k \in 1,2 , \qquad (2)$$

respectively. Using the two phase indicator functions defined as

$$X_k(\mathbf{x},t) = \begin{cases} 1 & ,\mathbf{x} \in \Omega_k(t) \\ 0 & ,\text{else,} \end{cases} \qquad\qquad (3)$$

yields the volume fraction of phase *k* within volume *V* as

$$\alpha_k \equiv \frac{1}{V} \int_V X_k(\mathbf{x} + \mathbf{\eta}, t) \, d\mathbf{x_\eta} = \frac{V_k}{V}. \tag{4}$$

The volume averaging operator for a general scalar or vector quantity, ψ_k, over the entire volume V and over the volume , V_k, occupied solely by phase k, respectively, are defined as

$$\overline{\psi}_k^V \equiv \frac{1}{V} \int_V \psi_k(\mathbf{x} + \mathbf{\eta}, t) X_k(\mathbf{x} + \mathbf{\eta}, t) \, d\mathbf{x_\eta}, \quad \overline{\psi}_k^k \equiv \frac{1}{V_k} \int_V \psi_k(\mathbf{x} + \mathbf{\eta}, t) X_k(\mathbf{x} + \mathbf{\eta}, t) \, d\mathbf{x_\eta}. \tag{5}$$

For each phase k, these averages are linearly related to one another through the respective volume fraction, namely:

$$\overline{\psi}_k^V = \alpha_k \overline{\psi}_k^k. \tag{6}$$

In this paper, we consider incompressible fluids only, as is also the case with all of the current VOF computations, so that the densities ρ_1 and ρ_2 will henceforth be assumed constant. Introducing this assumption in Eqs. (1) and (2), multiplying each of these equations by the respective phase indicator function, performing the average over V, and applying the Gauss and Leibniz rules, respectively, yields

$$\frac{\partial \alpha_k \rho_k}{\partial t} + \nabla \cdot \alpha_k \rho_k \overline{\mathbf{v_k}}^k = 0, \tag{7}$$

$$\frac{\partial \alpha_k \rho_k \overline{\mathbf{v_k}}^k}{\partial t} + \nabla \cdot \alpha_k \rho_k \overline{\mathbf{v_k} \mathbf{v_k}}^k = -\nabla \alpha_k \overline{p}_k^k + \alpha_k \rho_k \mathbf{g} + \nabla \cdot \alpha_k \overline{\mathbf{\tau_k}}^k + \mathbf{M_k}. \tag{8}$$

Note that the field equations (7) and (8) are valid in the entire domain Ω.

The term $\mathbf{M_k}$ appearing in Eq. (8) is the momentum transfer across the interface. When the coefficient of surface tension, σ, is constant, the terms $\mathbf{M_k}$ satisfy the jump condition

$$\mathbf{M}_1 + \mathbf{M}_2 = \mathbf{m}_i^\sigma = \frac{\sigma}{V} \int_{S_i(\mathbf{x},t)} \kappa \mathbf{n} \, dS, \tag{9}$$

where $S_i(\mathbf{x},t)$ denotes the interface position, κ is the mean curvature, and $\mathbf{n}$ is the unit normal vector to the interface.

The motion of the interface or turbulence may introduce velocity fluctuations in each fluid. We account for these local deviations from the mean value by introducing the fluctuating velocity field

$$\mathbf{v_k}' \equiv \mathbf{v_k} - \overline{\mathbf{v_k}}^k. \tag{10}$$

Due to the non-linear convective term, this decomposition gives rise to a sub-grid stress (sgs) term in the momentum equation (8), namely:

$$\alpha_k \rho_k \overline{\mathbf{v_k} \mathbf{v_k}}^k = \alpha_k \rho_k \overline{\mathbf{v_k}}^k \overline{\mathbf{v_k}}^k - \alpha_k \mathbf{\tau}_{sgs}^k, \quad \text{where} \quad \mathbf{\tau}_{sgs}^k \equiv -\rho_k \overline{\mathbf{v_k}' \mathbf{v_k}'}^k. \tag{11}$$

3. Volume-averaged single-field equations

This section outlines the derivations leading to the new single-field formulation for the governing equations. Thus, subsection 3.1 presents the volume-averaged single-field mass conservation equation, while subsection 3.2 presents the volume-averaged single-field momentum conservation equation. In subsection 3.3, we derive a volume-averaged transport equation for the liquid volumetric fraction which is needed to track the interface in the VOF method. These derivations follow largely the work of Sabisch (2000). Note that the notations α_1 and f for the liquid volume fraction, and α_2 and $(1-f)$ for the gas volume fraction, respectively will be interchangeably used in the sequel.

3.1. Volume-averaged single-field mass conservation equation

The volume-averaged mass conservation equations (7) are summed over both phases to obtain

$$\frac{\partial}{\partial t}\sum_{k=1}^{2}\alpha_k\rho_k + \nabla\cdot\sum_{k=1}^{2}\alpha_k\rho_k\overline{\mathbf{v_k}}^{k} = 0. \tag{12}$$

Defining a mixture density, ρ_m, and a center-of-mass velocity, $\mathbf{v_m}$, respectively, as

$$\rho_m \equiv \sum_{k=1}^{2}\alpha_k\rho_k = f\rho_1 + (1-f)\rho_2, \quad \mathbf{v_m} \equiv \frac{1}{\rho_m}\sum_{k=1}^{2}\alpha_k\rho_k\overline{\mathbf{v_k}}^{k} = \frac{f\rho_1\overline{\mathbf{v}_1}^{1} + (1-f)\rho_2\overline{\mathbf{v}_2}^{2}}{\rho_m}, \tag{13}$$

and introducing these definitions in Eq. (12) reduces it to the following compact form:

$$\frac{\partial\rho_m}{\partial t} + \nabla\cdot\rho_m\mathbf{v_m} = 0, \tag{14}$$

which has the same conservation form as for single-phase flow but where the single-phase density and velocity are replaced by the mixture density and the center-of-mass velocity, respectively.

3.2. Volume-averaged single-field momentum equation

Summing the averaged momentum equations (8) for both phases, and introducing the jump condition due to equation (9) yields:

$$\frac{\partial}{\partial t}\sum_{k=1}^{2}\alpha_k\rho_k\overline{\mathbf{v_k}}^{k} + \nabla\cdot\sum_{k=1}^{2}\alpha_k\rho_k\overline{\mathbf{v_k}}^{k}\overline{\mathbf{v_k}}^{k} = -\nabla\sum_{k=1}^{2}\alpha_k\overline{p_k}^{k} + \sum_{k=1}^{2}\alpha_k\rho_k\mathbf{g}$$

$$+ \nabla\cdot\sum_{k=1}^{2}\alpha_k(\overline{\boldsymbol{\tau_k}}^{k} + \boldsymbol{\tau_{sgs}^{k}}) + \frac{\sigma}{V}\int_{S_i(\mathbf{x},t)}\kappa\mathbf{n}\,dS. \tag{15}$$

To rearrange the convective term into a compact form, it is convenient to define the *local phase-space-averaged relative velocity*

$$\mathbf{v_r} \equiv \overline{\mathbf{v_2}}^{2} - \overline{\mathbf{v_1}}^{1}, \tag{16}$$

which provides a measure of the velocity difference between the phases within the averaging volume V. Using Eq. (16), the convective term is now written as the sum of two terms, one depending on the center-of-mass velocity, $\mathbf{v_m}$, and another one depending on the relative velocity $\mathbf{v_r}$:

$$\sum_{k=1}^{2}\alpha_k\rho_k\overline{\mathbf{v_k}}^{k}\overline{\mathbf{v_k}}^{k} = \rho_m\mathbf{v_m}\mathbf{v_m} + \mathbf{D_{int}}, \quad \text{where} \quad \mathbf{D_{int}} \equiv \alpha_1\alpha_2\frac{\rho_1\rho_2}{\rho_m}\mathbf{v_r}\mathbf{v_r}. \tag{17}$$

Equation (17) shows that the term $\mathbf{D_{int}}$ expresses the difference between the total momentum flux and the average flux of the averaged momentum. Therefore, we refer to this term as *momentum drift-flux term* (MDF term).

The next step is to split the term $\sum_{k=1}^{2}\alpha_k\overline{\boldsymbol{\tau_k}}^{k}$, too, into two terms that depend on, $\mathbf{v_m}$, and on $\mathbf{v_r}$, respectively. For this purpose, we use the constitutive equation for viscous stress for incompressible Newtonian fluids, namely

$$\boldsymbol{\tau_k} = \mu_k(\nabla\mathbf{v_k} + \nabla\mathbf{v_k}^{T}), \tag{18}$$

assume that the viscosity μ_k is constant for each phase, average over the volume V_k, and introduce in the above sum to obtain

$$\sum_{k=1}^{2} \alpha_k \overline{\boldsymbol{\tau}_{\mathbf{k}}}^{k} = \sum_{k=1}^{2} \alpha_k \mu_k \left(\nabla \overline{\mathbf{v}_{\mathbf{k}}}^{k} + \nabla \overline{\mathbf{v}_{\mathbf{k}}}^{k\,\mathrm{T}} \right) \equiv \boldsymbol{\tau}_{\mathbf{m}} + \boldsymbol{\tau}_{\mathbf{int}} \,, \tag{19}$$

where

$$\boldsymbol{\tau}_{\mathbf{m}} \equiv \mu_m (\nabla \mathbf{v}_{\mathbf{m}} + \nabla \mathbf{v}_{\mathbf{m}}^{\mathrm{T}}), \quad \mu_m \equiv f\mu_1 + (1 - f)\mu_2 \,, \tag{20}$$

and $\boldsymbol{\tau}_{\mathbf{int}}$ remains to be calculated below. For this purpose, we write the center-of-mass velocity in the form

$$\mathbf{v}_{\mathbf{m}} = \frac{\alpha_1 \rho_1 \overline{\mathbf{v}_{\mathbf{1}}}^{1} + \alpha_2 \rho_2 \overline{\mathbf{v}_{\mathbf{2}}}^{2}}{\alpha_1 \rho_1 + \alpha_2 \rho_2} = \overline{\mathbf{v}_{\mathbf{1}}}^{1} + \overline{\mathbf{v}_{\mathbf{2}}}^{2} - \mathbf{w}, \quad \text{where} \quad \mathbf{w} \equiv \frac{\alpha_1 \rho_1 \overline{\mathbf{v}_{\mathbf{2}}}^{2} + \alpha_2 \rho_2 \overline{\mathbf{v}_{\mathbf{1}}}^{1}}{\alpha_1 \rho_1 + \alpha_2 \rho_2} \,, \tag{21}$$

and replace in Eq. (20) to obtain

$$\begin{aligned}
\boldsymbol{\tau}_{\mathbf{m}} &= \alpha_1 \mu_1 \left(\nabla \overline{\mathbf{v}_{\mathbf{1}}}^{1} + \nabla \overline{\mathbf{v}_{\mathbf{1}}}^{1\,\mathrm{T}} \right) + \alpha_2 \mu_2 \left(\nabla \overline{\mathbf{v}_{\mathbf{2}}}^{2} + \nabla \overline{\mathbf{v}_{\mathbf{2}}}^{2\,\mathrm{T}} \right) \\
&\quad + \alpha_1 \mu_1 \left[\nabla (\overline{\mathbf{v}_{\mathbf{2}}}^{2} - \mathbf{w}) + \nabla (\overline{\mathbf{v}_{\mathbf{2}}}^{2} - \mathbf{w})^{\mathrm{T}} \right] + \alpha_2 \mu_2 \left[\nabla (\overline{\mathbf{v}_{\mathbf{1}}}^{1} - \mathbf{w}) + \nabla (\overline{\mathbf{v}_{\mathbf{1}}}^{1} - \mathbf{w})^{\mathrm{T}} \right].
\end{aligned} \tag{22}$$

Noting from Eq. (21) that

$$\overline{\mathbf{v}_{\mathbf{1}}}^{1} - \mathbf{w} = -\frac{\alpha_1 \rho_1}{\rho_m} \mathbf{v}_{\mathbf{r}}, \quad \overline{\mathbf{v}_{\mathbf{2}}}^{2} - \mathbf{w} = \frac{\alpha_2 \rho_2}{\rho_m} \mathbf{v}_{\mathbf{r}} \,, \tag{23}$$

replacing the above expressions in Eq. (22), and comparing the resulting expression with Eq. (19) shows that

$$\boldsymbol{\tau}_{\mathbf{int}} \equiv \sum_{k=1}^{2} \alpha_k \overline{\boldsymbol{\tau}_{\mathbf{k}}}^{k} - \boldsymbol{\tau}_{\mathbf{m}} = \alpha_2 \mu_2 \left(\nabla \frac{\alpha_1 \rho_1}{\rho_m} \mathbf{v}_{\mathbf{r}} + \nabla \frac{\alpha_1 \rho_1}{\rho_m} \mathbf{v}_{\mathbf{r}}^{\mathrm{T}} \right) - \alpha_1 \mu_1 \left(\nabla \frac{\alpha_2 \rho_2}{\rho_m} \mathbf{v}_{\mathbf{r}} + \nabla \frac{\alpha_2 \rho_2}{\rho_m} \mathbf{v}_{\mathbf{r}}^{\mathrm{T}} \right). \tag{24}$$

Since tensor $\boldsymbol{\tau}_{\mathbf{int}}$ arises from viscous forces, we shall refer to it as the *interfacial friction term*. Note that the elements of the tensor $\boldsymbol{\tau}_{\mathbf{int}}$ differ from zero only close to the interface.

We now consider the last term on the right-side of Eq. (15), which is due to surface tension. We approximate the respective integral as follows:

$$\frac{\sigma}{V} \int_{S_i(\mathbf{x},t)} \kappa \mathbf{n} \, dS \cong \sigma \, \overline{\kappa}^{V} \overline{\mathbf{n}}^{V} \frac{1}{V} \int_{S_i(\mathbf{x},t)} dS = \sigma \, \overline{\kappa}^{V} \overline{\mathbf{n}}^{V} a_{int} \,, \tag{25}$$

where $\overline{\kappa}^{V}$ is the mean curvature of the interface within V, $\overline{\mathbf{n}}^{V}$ is the mean unit normal vector to the interface within V, and a_{int} is the interfacial area concentration.

Replacing Eqs. (13), (17), (20), (24), and (25) in Eq. (15) yields the following form for the volume-averaged single-field Navier-Stokes equation:

$$\begin{aligned}
\frac{\partial \rho_m \mathbf{v}_{\mathbf{m}}}{\partial t} + \nabla \cdot \left(\rho_m \mathbf{v}_{\mathbf{m}} \mathbf{v}_{\mathbf{m}} + \mathbf{D}_{\mathbf{int}} \right) &= -\nabla \sum_{k=1}^{2} \alpha_k \overline{p_k}^{k} + \rho_m \mathbf{g} + \sigma \overline{\kappa}^{V} \overline{\mathbf{n}}^{V} a_{int} + \nabla \cdot \mu_m \left(\nabla \mathbf{v}_{\mathbf{m}} + \nabla \mathbf{v}_{\mathbf{m}}^{\mathrm{T}} \right) \\
&\quad + \nabla \cdot \left(\boldsymbol{\tau}_{\mathbf{int}} + \boldsymbol{\tau}_{\mathbf{sgs}} \right), \quad \text{where} \quad \boldsymbol{\tau}_{\mathbf{sgs}} = \sum_{k=1}^{2} \alpha_k \boldsymbol{\tau}_{\mathbf{sgs}}^{\mathbf{k}} = -\sum_{k=1}^{2} \alpha_k \rho_k \overline{\mathbf{v}_{\mathbf{k}}' \mathbf{v}_{\mathbf{k}}'}^{k}.
\end{aligned} \tag{26}$$

At this point, we remark that Eq. (26) obtained in the classical manner described in this section can also be obtained by averaging the local instant two-phase field equations of Kataoka (1986, formula 14 and 26, respectively) over a volume V.

3.3. *Volume-averaged conservation equation for the liquid volumetric fraction*

By using Eqs. (13) and (16), we first express each of the phase velocities as the sum of the center-of-mass velocity and the respective phase drift velocity, in the form

$$\overline{\mathbf{v}_1}^1 = \mathbf{v_m} - \frac{\alpha_2 \rho_2}{\rho_m}\mathbf{v_r}, \quad \overline{\mathbf{v}_2}^2 = \mathbf{v_m} + \frac{\alpha_1 \rho_1}{\rho_m}\mathbf{v_r}, \tag{27}$$

and use the above results in Eq. (7), i.e., the mass conservation equation for phase k, to obtain

$$\frac{\partial f\rho_1}{\partial t} + \nabla \cdot f\rho_1 \mathbf{v_m} = \nabla \cdot f(1-f)\frac{\rho_1 \rho_2}{\rho_m}\mathbf{v_r}, \qquad \text{for } k=1, \text{ and} \tag{28}$$

$$\frac{\partial(1-f)\rho_2}{\partial t} + \nabla \cdot (1-f)\rho_2 \mathbf{v_m} = -\nabla \cdot f(1-f)\frac{\rho_1 \rho_2}{\rho_m}\mathbf{v_r}, \text{ for } k=2. \tag{29}$$

For numerical computations with the VOF-method, Ghidersa (2000) observed that it is convenient to rearrange the above equations into the following forms:

$$\frac{\partial f}{\partial t} + \nabla \cdot f\mathbf{v_m} = \nabla \cdot f(1-f)\frac{\rho_2}{\rho_m}\mathbf{v_r}, \tag{30}$$

and

$$\nabla \cdot \mathbf{v_m} = -\nabla \cdot f(1-f)\frac{\rho_1 - \rho_2}{\rho_m}\mathbf{v_r}. \tag{31}$$

The set of equations consisting of (i) the momentum equation (26), (ii) the transport equation (30) for the liquid volumetric fraction, and (iii) the divergence condition for the center-of-mass velocity derived in Eq. (31), will henceforth be referred to as the set of *volume averaged (VA) VOF equations*. Note that this is *a set of three equations with five unknowns,* namely $\mathbf{v_m}$, $\mathbf{v_r}$, f, $\overline{p_1}^1$, and $\overline{p_2}^2$, and is therefore incomplete at this stage. The closure of these VA-VOF equations will be accomplished in section 5, below, by (i) introducing a new model for $\mathbf{v_r}$, and (ii) assuming, as is customary for two-phase flows, that both phases are subject to the same pressure field.

4. Comparison of the VA-VOF equations with the local-VOF equations

4.1. Differential VA-VOF and local-VOF equations

The VA-VOF equations (26), (30), and (31) are formulated in terms of the center-of-mass velocity, $\mathbf{v_m}$, and the local phase-space-averaged relative velocity, $\mathbf{v_r}$. In single-phase regions (i.e., for $f = 0$ or $f = 1$), though, the VA-VOF equations reduce, as they should, to those for a single fluid, with the appropriate density and viscosity. On the other hand, Eqs. (14), (26), and (29) have the same appearance as those underlying the three-dimensional drift-flux model (Ishii, 1975). Note, though, that the latter equations were derived by Ishii (1975) using time-averages, while we derived Eqs. (14), (26), and (29) using volume-averages.

The equations underlying the *local-VOF* method are the *local* single-field Navier-Stokes and continuity equations, and the transport equation for the liquid volumetric fraction, f. Both the conservative and non-conservative forms of these equations are used in practice. Without loss of generality, we shall use for our comparative discussion the conservative forms, written as

$$\frac{\partial \rho_m \mathbf{v}}{\partial t} + \nabla \cdot \rho_m \mathbf{v}\mathbf{v} = -\nabla p + \nabla \cdot \mu_m(\nabla \mathbf{v} + \nabla \mathbf{v}^T) + \rho_m \mathbf{g} + \sigma \kappa \mathbf{n}\delta_S, \tag{32}$$

$$\nabla \cdot \mathbf{v} = 0, \tag{33}$$

where δ_S is a surface delta function, and the *local f*-equation, written as

$$\frac{\partial f}{\partial t} + \nabla \cdot f \mathbf{v} = 0 \,. \tag{34}$$

It is important to note that these "local"-VOF equations, as have been used in the literature so far, are *inconsistent* in the sense that although some of the quantities appearing in them are local, the quantities f, ρ_m and μ_m are not, since they already represent volume averages. Therefore, the local-VOF equations are appropriate only when the control volume is sufficiently small so that both phases move with the same velocity. If there exist velocity fluctuations within a control volume, the local-VOF equations become incomplete, since these fluctuations give rise to one additional unknown. This fact is apparent in the newly derived VA-VOF equations (26), (30), and (31) which contain the additional unknown $\mathbf{v_r}$. Note that $\mathbf{v_r}$ is non-zero only in RVE's that contain both phases, which occurs only close to the interface. In the limit of vanishingly small $\mathbf{v_r}$, which occurs under the "homogeneous model" assumption or in the limit of vanishingly small RVE's, the VA-VOF equations reduce to the local-VOF equations.

4.2. Discretized VA-VOF and local-VOF equations

The volume-averaging inherent to the VA-VOF equations is equivalent to a local 3D-filtering in the physical space, and is therefore conceptually related to the Large Eddy Simulation (LES) methods. In the framework of LES methods for *single-phase flows*, the type of the filter and the width of the filter, Δ, may be selected independently of one another as long as the grid size, h, fulfills the condition that $h \leq \Delta$ (see, e.g., Ferziger and Peric, 1996). Usually, Δ is chosen to be about one to four times the mesh size h. For *two-phase flows*, however, the VOF method uses the liquid volumetric fraction f for reconstructing and tracking the interface, which implies that the filter is a box filter of width $\Delta = h$. This intimate relationship between the numerical discretization and the smoothing of the flow variables is an inherent characteristic of the VA-VOF method, as it also is in the method of Schumann (1975) for single-phase LES.

By including the subgrid stress term due to unresolved velocity fluctuations in the single-field VA-VOF momentum equation (26), we provide a framework for using this method to perform LES of interfacial flows. Thus, while the interface segment that is well resolved by the grid is reconstructed explicitly, the effects of the unresolved interfacial boundary layers and unresolved velocity fluctuations can be included in models for $\mathbf{v_r}$ and $\boldsymbol{\tau_{sgs}}$, respectively.

In the VA-VOF Eqs. (26), (30) and (31), the divergence operator is applied to all terms involving $\mathbf{v_r}$. Thus, the divergence operator and the model for $\mathbf{v_r}$ must be discretized consistently to ensure that the momentum and the mass of each phase are globally conserved. Nevertheless, the modeling of $\mathbf{v_r}$ affects the local conservation of mass and momentum within a RVE. Note that the discretization of the divergence operator causes the effects of the closure terms to extend beyond the RVE's containing two-phases, affecting the RVE's adjacent to the interface.

We will now discuss the treatment of the surface tension in the local-VOF equation (32) and our VA-VOF equation (26). In the local-VOF methods, the surface tension is treated as a volume force, which is modeled as a Continuum Surface Force (CSF), Brackbill et al. (1992), or as a Continuos Surface Stress (CSS), Lafauri et al. (1994). In both models, the interfacial tension force is no longer concentrated at the interface, as the surface delta function would suggest, but is smeared over a distance of roughly the size of a mesh-cell. In the CSF model, for example, the interface unit normal vector $\mathbf{n}$ and the curvature κ are computed using the formulas

$$\mathbf{n} = \frac{\nabla f}{|\nabla f|}, \quad \kappa = -\nabla \cdot \mathbf{n} \,. \tag{35}$$

Since f is discontinuous across the interface, it is usually replaced in Eq. (35) by a *smoothed* volume fraction, defined as the convolution between f and a smoothing kernel; the optimal representation of which is still a topic of intense research (Williams et al., 1999).

In contradistinction with the CSF method, however, in our VA-VOF formulation, the surface tension force in Eq. (25) already represents an averaging over the volume *V*. Thus, volume-smoothing is inherent to our VA-VOF representation of surface tension. Furthermore, the degree of smoothing in the VA-VOF is determined by the averaging volume *V*, rather than by an arbitrary kernel as in the CSF model. Nevertheless, the RVE must be sufficiently small in order to resolve the interface curvature sufficiently well for meaningful approximations by mean values of **n** and κ in Eq. (25).

In a companion paper (Sabisch et al. 2001, this conference), we illustrate the discretization of the surface tension term, cf. Eq. (25), on a staggered grid. There, we used the interface normal, **n**, obtained from our VOF reconstruction algorithm, called EPIRA, instead using Eq. (35). The accuracy of this procedure was verified using several representative test problems and was successfully used to simulate bubbles of steady and non-steady shape rising in a continuous liquid.

5. Modeling the local phase-space-averaged relative velocity $\mathbf{v_r}$

5.1. A local algebraic model for the relative velocity $\mathbf{v_r}$

To obtain the relative velocity $\mathbf{v_r} = (u_r, v_r, w_r)^T$, we need to determine the individual phase velocities, as illustrated on the staggered grid shown in Fig. 1, below, which shows three neighboring cells centered at *i-1*, *i*, and *i+1*, respectively, along a co-ordinate direction. Note that the components of $\mathbf{v_r}$ will be defined at the center *i*, in order to ensure that the divergence operator is discretized consistently, as discussed above, in section 4.2.

The component u_r of $\mathbf{v_r}$ at position *i* is obtained from its definition, namely Eq. (16), which yields $u_{r;i} = u_{2;i} - u_{1;i}$. Note that the overbars have been omitted for notational simplicity. The components $u_{1;i}$ and $u_{2;i}$ are obtained by (i) using the definition given in Eq. (13) for the component u_m of $\mathbf{v_m}$, namely

$$u_{m;i\pm1/2} = \frac{f_{i\pm1/2}\rho_1 u_{1;i\pm1/2} + \left(1 - f_{i\pm1/2}\right)\rho_2 u_{2;i\pm1/2}}{\rho_{m;i\pm1/2}}, \tag{36}$$

and (ii) assuming that within the dashed region in Fig. 1 (i.e. the staggered control volume of the first component of the momentum equation), the respective velocity component of both the gas and liquid phases are uniform, namely:

$$u_{1;i+1/2} = u_{1;i-1/2} = u_{1;i}, \quad u_{2;i+1/2} = u_{2;i-1/2} = u_{2;i}. \tag{37}$$

After considerable algebraic manipulations, the above sequence of steps yields

$$u_{r;i} = -\left(1 + \frac{\rho_1 - \rho_2}{\rho_2}f_{i-1/2}\right)\left(1 + \frac{\rho_1 - \rho_2}{\rho_2}f_{i+1/2}\right)\frac{\rho_2}{\rho_1}\frac{u_{m;i+1/2} - u_{m;i-1/2}}{f_{i+1/2} - f_{i-1/2}}. \tag{38}$$

Equation (38) is valid only when $f_{i+1/2} \neq f_{i-1/2}$. Otherwise, Eq. (38) is singular; in this case, we set u_r to zero, which is equivalent to assuming that both phases flow with the same velocity in the respective direction.

The other components of $\mathbf{v_r}$ are obtained following the same conceptual steps as for obtaining u_r in Eq. (38). The resulting model for $\mathbf{v_r}$ will be referred to in the remaining of this paper as the *local* (as opposed to global) *uniform relative velocity (LURV) model*.
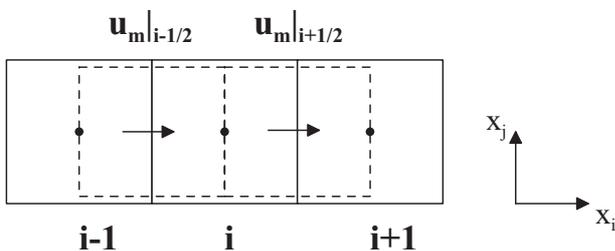
Fig. 1:
Staggered grid for calculating the component u_r in cell *i*, showing the centered (solid line) and staggered (dashed line) RVE's.

5.2. Results for a cylindrical interface at rest

This section presents simulations using the VA-VOF equations as implemented in our computer code TURBIT-VOF (Sabisch, 2000; Sabisch et al., 2001) for a cylindrical interface between two immiscible fluids. Both fluids have the same density and viscosity and are initially at rest; the surface tension is the only driving force in the system. Based on physical considerations, the system should remain in static equilibrium. However, the numerical simulation usually introduce unphysical velocities across the interface, known as *parasitic* or *spurious currents* (Lafaurie et al., 1994; Popinet and Zaleski, 1999). We also note here that all of the simulations reported in the literature to date for this problem have been performed in 2D only. For comparison purposes, therefore, we needed to adapt our 3D code to the respective 2D geometry, by applying periodic boundary conditions in one co-ordinate direction (here x_2) and using only four mesh cells within this direction.

In our simulations, we used the LURV model only within the momentum equation (26), to model $\mathbf{D_{int}}$ and $\mathbf{\tau_{int}}$. For the transport equation for f, and for the divergence condition for the center-of-mass velocity, i.e., Eqs. (30) and (31), we used the homogeneous model in order to avoid affecting the local mass conservation within each RVE. Our TURBIT-VOF code is based on non-dimensional equations. For the simulations described below, the length scale is $L_{ref} = 4$m and the velocity scale is $U_{ref} = 1$ms^{-1}. The relevant non-dimensional numbers are the reference Reynolds number, $Re_{ref} = \rho_1 L_{ref} U_{ref} / \mu_1$, and the reference Weber number, $We_{ref} = \rho_1 L_{ref} U^2_{ref} / \sigma$; in the simulations, we use $Re_{ref} = 20$ and $We_{ref} = 40$. The nominal non-dimensional pressure difference due to Laplace's law is $\Delta p = H/We_{ref} = 0.1$, where H is the non-dimensional interface curvature. The non-dimensional size of the computational domain is $1 \times 4\Delta x \times 1$. In addition to x_2, we also use periodic boundary conditions in the x_1-direction, and use a no-slip condition in the x_3-direction. The numerical simulations are performed for three different grids consisting of 20×4×20, 40×4×40, and 80×4×80 uniform cells, respectively. This yields a resolution of the diameter of the cylindrical interface by 10, 20, and 40 mesh cells, respectively. For these conditions, H has the value 4.

Figure 2 shows the time evolution of the non-dimensional maximum velocity, u_{max}, computed with the homogeneous model and with the LURV model in the VA-VOF momentum equation, respectively. Although the results for the initial transient evolution of u_{max} are grid-dependent, the steady state value calculated for u_{max} is almost independent of grid resolution. As displayed in Fig. 2, the use of the LURV model in the momentum equation reduces u_{max} by about 30% by comparison to using the homogeneous model. Note, however, that none of the simulations attained the exact solution $u_{max} = 0$, and grid refinements have even failed to reduce substantially the value of u_{max}. This is because, on the one hand, refining the grid leads to a more accurate computation of the interface normal vector, $\mathbf{n}$, and the curvature, κ. On the other hand, however, this refinement leads to an increase of the interfacial area concentration, a_{int}, since a_{int} is inversely proportional to the size of a mesh cell. Note that Popinet and Zaleski (1999) also observed, in their VOF computations, that the amplitude of the spurious currents is almost independent of the spatial resolution. By contrast, when they performed simulations with a marker-based front-tracking method using an empirical correction for computing the pressure gradient across the interface, they were able to reduce the spurious currents amplitude drastically as compared to the VOF method. With this front-tracking method they also obtained a reduction of the spurious currents amplitude when increasing the grid resolution.

In addition to the simulations presented above with $\Delta p = 0.1$, we also performed simulations with $\Delta p = 1$ and $\Delta p = 10$, where $We_{ref} = 4$ and 0.4 is used, respectively . We observed that, for all these runs, the computed difference between the pressures inside and outside the cylindrical interface differs by less than 1% from the exact value predicted by Laplace's law. In the simulations using the LURV model with $\Delta p = 1$ and $\Delta p = 10$, we have also observed a reduction of u_{max} by about 30% by comparison to the homogeneous model (Sabisch, 2000). Although these simulations have not always yielded a constant value for u_{max}, the asymmetries of the cylindrical interfaces were small.
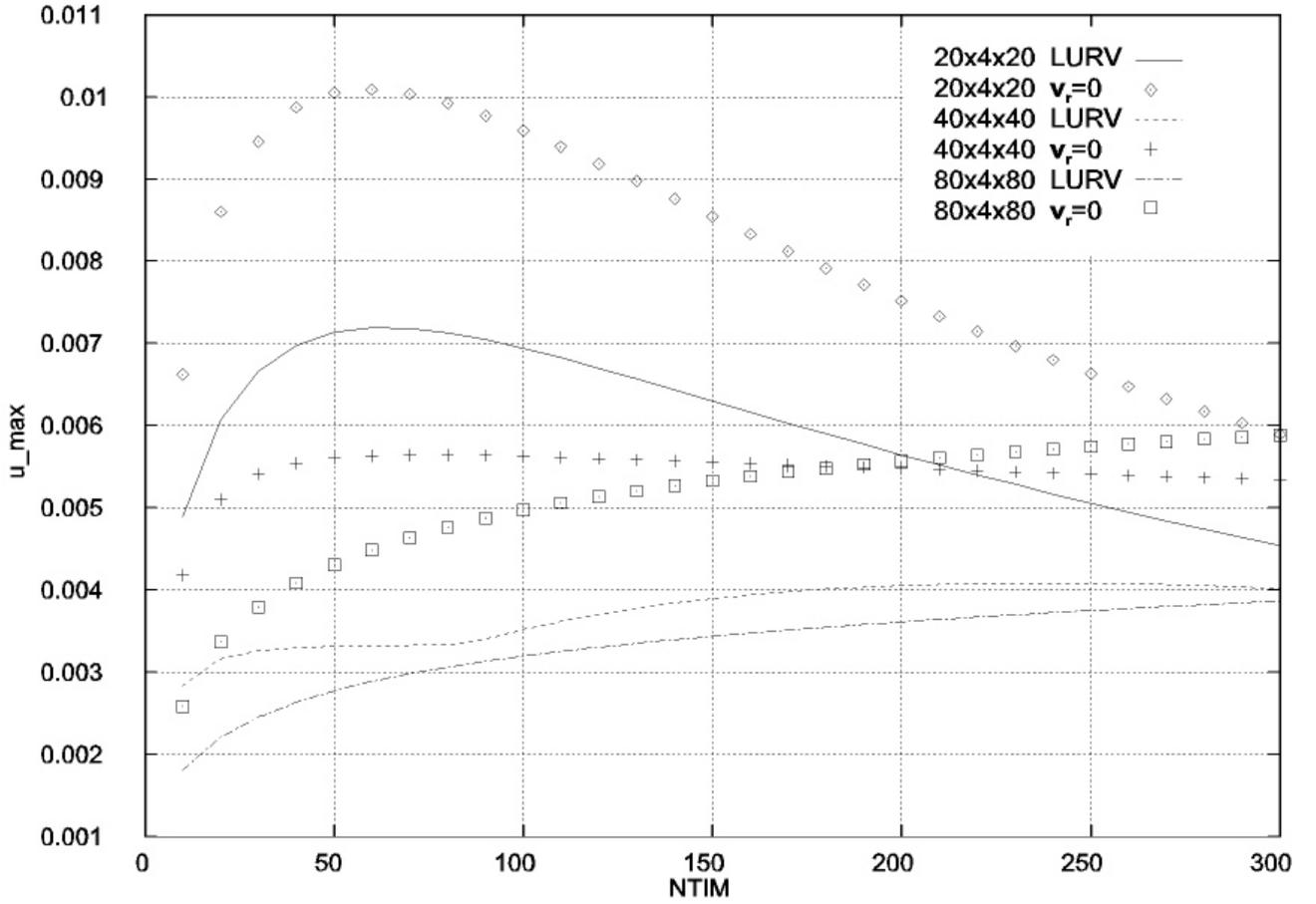
Fig. 2: Temporal evolution of the non-dimensional velocity amplitude, u_{max}, due to spurious currents (NTIM is the number of time steps), for the homogeneous model (symbols) and the LURV model (lines), using three different grids in each case.

6. Summary and conclusions

In this paper, we have outlined the derivations of locally volume-averaged single-field conservation equations, namely Eqs. (26), (30), and (31), for a two-phase system consisting of two immiscible incompressible components. These equations are suitable for coarse-grid numerical simulations, e.g. with the Volume-of-Fluid (VOF) method, of dynamic interface evolutions. We call Eqs. (26), (30), and (31) the *set of volume-averaged VOF equations* (VA-VOF). As compared to the local single-field equations currently used with the VOF method, the newly derived VA-VOF equations contain additional terms which depend on the local phase-space-averaged relative velocity of the individual phases, $\mathbf{v_r}$, defined in Eq. (16). These additional terms are: (i) $\mathbf{D_{int}}$, defined in Eq. (17), which expresses the difference between the total momentum flux and the average flux of the averaged momentum, and which is therefore referred to as *momentum drift-flux term* (MDF term), (ii) the tensor $\boldsymbol{\tau_{int}}$, defined in Eq. (24), which arises from viscous forces, and is therefore referred to as the *interfacial friction term,* and (iii) the terms on the right-side of Eqs. (30) and (31). These terms represent the influence of velocity fluctuations close to the interface in the respective equation.

We have noted that the VA-VOF system is not closed, and a model assumption for $\mathbf{v_r}$ is needed to close it. We have also noted, though, that this closure problem is relevant only for mesh cells that instantaneously contain both phases. In three-dimensional VA-VOF computations, this problem affects typically less than 1% of the total number of mesh cells. In the limit of very fine computational grids, or by introducing the "homogeneous model" (i.e. $\mathbf{v_r} = 0$) in our set of VA-VOF

equations, we recover the local form of the VOF-equations (as used in current code implementations).

While the "homogeneous model" may be justified for VOF computations on very fine grids, the modeling of the relative velocity $\mathbf{v_r}$ may nevertheless become important. For this purpose, we have presented a local algebraic model for $\mathbf{v_r}$, called the local uniform relative velocity (LURV) model. We have then used this model for the momentum drift-flux term, $\mathbf{D_{int}}$, and the interfacial friction term, $\mathbf{\tau_{int}}$, respectively. Finally, we presented results from VA-VOF simulations for a cylindrical interface, initially in static equilibrium. These results showed that the negative effects of spurious currents, which numerically corrupt the physically static interface, is reduced by about 30%.

The use of the set of volume-averaged single-field equations derived in this paper is not restricted to the VOF technique for interface tracking. In principle, this set of equations can also be used in combination with the level-set method. We also note that the VA-VOF set of equations might provide a basis for "large-eddy" two-phase simulations with interface tracking, where the unresolved boundary layer close to the interface can be included in the modeling of $\mathbf{v_r}$, while the unresolved velocity fluctuations can be included in the modeling of two-phase subgrid-scale effects.

References

Brackbill, J.U., Kothe, D.B., Zemach, C., 1992. A Continuum Method for Modeling Surface Tension. J. Comput. Phys. 100, 335-354.

Bussmann, M., Mostaghimi, J., Chandra, S., 1999. On a three-dimensional volume tracking model of droplet impact. Physics of Fluids 11, 1406-1417.

Chen, L., Garimella, S.V., Reizes, J.A., Leonardie, E., 1999. The development of a bubble rising in a viscous liquid. J. Fluid Mech. 387, 61-96.

Drew, D.A., Passmann, S.L., 1999. Theory of Multicomponent Fluids. Applied Mathematical Sciences Vol. 135, Springer.

Ferziger, J.H., Perić, M., 1996. Computational Methods for Fluid Dynamics. Springer.

Ghidersa, B., 2000. Unpublished report, Forschungszentrum Karlsruhe.

Gueyffier, D., Li, J., Scardovelli, R., Zaleski, S., 1999. Volume-of-Fluid Interface Tracking with Smoothed Surface Stress Methods for Three-Dimensional Flows. J. Comput. Phys. 152, 423-456.

Hirt, C.W., Nichols, B.D., 1981. Volume of Fluid (VOF) method for the dynamics of free boundaries. J. Comput. Phys. 39, 201-225.

Ishii, M., 1975. Thermo-Fluid Dynamic Theory of Two-Phase Flow. Eyrolles, Paris.

Kataoka, I., 1986. Local instant formulation of two-phase flow. Int. J. Multiphase Flow 12, 745-758.

Kothe, D.B., 1998. Perspective on Eulerian Finite Volume Methods for Incompressible Interfacial Flows. In: Free Surface Flows. H.C. Kuhlmann, H-J Rath, Editors. Springer-Verlag, 267-331.

Lafauri, B., Nardone, C., Scardovelli, R., Zaleski, S., 1994. Modelling Merging and Fragmentation in Multiphase Flows with SURFER. J. Comput. Phys. 113, 134-147.

Lawson, N.J., Rudman, M., Guerra, A., Liow, J.-L., 1999. Experimental and numerical comparisons of the break-up of a large bubble. Experiments in Fluids 26, 524-534.

Li, J., Renardy, Y., 2000. Numerical Study of Flows of Two Immiscible Liquids at Low Reynolds Number. SIAM Review 42, 417-439.

Meier, M., Yadigaroglu, G., 2000. Numerical and Experimental Study of large Steam-Air Bubbles Injected in a Water Pool. Nuclear Science and Engineering 136, 363-375.

Popinet, S., Zaleski, S., 1999. A front-tracking algorithm for accurate representation of surface tension. Int. J. Num. Meth. Fluids 30, 775-793.

Rider, W.J., Kothe, D.B., Puckett, E.G., Aleinov, I.D., 1998. Accurate and Robust Methods for Variable Density Incompressible Flows with Discontinuities. In: Barriers and Challenges in Computational Fluid Dynamics, V.Venkatakrishnan, M.D. Salas, and S.R. Chakravarthy, Editors. Kluwer Academic Publishers, Boston, 213-230.

Rieber, M., Frohn, A., 1999. A numerical study on the mechanism of splashing. Int. J. Heat and Fluid Flow 20, 455-461.

Sabisch, W., 2000. Dreidimensionale numerische Simulation der Dynamik von aufsteigenden Einzelblasen und Blasenschwärmen mit einer Volume-of-Fluid-Methode. Forschungszentrum Karlsruhe, Wissenschaftliche Berichte FZKA 6478, Juni 2000 (http://www.fzk.de/hbk/literatur/ FZKA_Berichte/FZKA6478.pdf).

Sabisch, W., Wörner, M., Grötzbach, G., Cacuci, D.G., 2001. 3D volume-of-fluid simulation of a wobbling bubble in a gas-liquid system of low Morton number. Proc. 4th Int. Conference on Multiphase Flow, ICMF-2001, New Orleans, Louisiana, U.S.A., May 27 - June 1, 2001.

Scardovelli, R., Zaleski, S., 1999. Direct numerical simulation of free-surface and interfacial flows. Annu. Rev. Fluid Mech. 31, 567-603.

Schumann, U., 1975. Subgrid Scale Model for Finite Difference Simulations of Turbulent Flows in Plane Channels and Annuli. J. Comput. Phys. 18, 376-404.

Welch, S.W.J., Wilson, J., 2000. A volume of fluid based method for fluid flows with phase change. J. Comput. Phys. 160, 662-682.

Williams, M.W., Kothe, D.B., Puckett E.G., 1999. Accuracy and Convergence of Continuum Surface-Tension Models. In: Fluid Dynamics at Interfaces, W. Shyy and R. Narayanan, Editors. Cambridge University Press, 1999.